Conformational Transitions of the Phosphodiester Backbone in Native DNA: Two-Dimensional Magic-Angle-Spinning ^{31}P-NMR of DNA Fibers

Zhiyan Song, Oleg N. Antzutkin, Young K. Lee, S. C. Shekar, Allan Rupprecht, and Malcolm H. Levitt
Division of Physical Chemistry, Arrhenius Laboratory, University of Stockholm, S-106 91 Stockholm, Sweden

ABSTRACT Solid-state ^{31}P-NMR is used to investigate the orientation of the phosphodiester backbone in NaDNA-, LiDNA-, MgDNA-, and NaDNA-netropsin fibers. The results for A- and B-DNA agree with previous interpretations. We verify that the binding of netropsin to NaDNA stabilizes the B form, and find that in NaDNA, most of the phosphate groups adopt a conformation typical of the A form, although there are minor components with phosphate orientations close to the B form. For LiDNA and MgDNA samples, on the other hand, we find phosphate conformations that are in variance with previous models. These samples display x-ray diffraction patterns that correspond to C-DNA. However, we find two distinct phosphate orientations in these samples, one resembling that in B-DNA, and one displaying a twist of the PO_4 groups about the O_3-P-O_4 bisectors. The latter conformation is not in accordance with previous models of C-DNA structure.

INTRODUCTION

It is well known that the DNA double helix adopts a variety of secondary structures, such as the right-handed A, B, and C forms, and the left-handed Z form (Saenger, 1984). These DNA conformations are characterized by different molecular structural parameters, such as the helical pitch, the axial rise per basepair, the groove size, the base tilt, the sugar puckering, and the orientation of the phosphate groups. The existence of a particular conformation depends on the DNA sequence and the environmental conditions, such as the relative humidity, the nature of the counterions, the salt concentration, and the binding of ligands (Saenger, 1984).

Most of our knowledge of DNA molecular structure derives from x-ray diffraction of oligonucleotide crystals and of fibers. The most precise information is obtained from x-ray crystallography of oligonucleotides, mainly in A, B, and Z forms or DNA-drug complexes (Heinemann et al., 1994; Wahl and Sundaralingam, 1995). However, this method is limited to rather short nucleotide sequences, and certain forms of DNA, such as the C form, have never been crystallized.

X-ray fiber diffraction patterns of DNA can be analyzed to obtain the helix parameters, such as the tilt of the base planes, the pitch of the helix, and the helix rise per basepair (Langridge et al., 1960; Marvin et al., 1961; Fuller et al., 1965; Arnott and Hukins, 1973). However, the information about the conformation of sugars and the phosphate backbone is limited by relatively poor resolution of x-ray fiber diffraction data, and is "model dependent" (Fuller et al., 1965; Arnott, 1980; Pohle et al., 1984). The method is difficult to apply if the sample consists of a mixture of different conformations, or if the crystallinity of DNA fibers is poor.

The combined limitation of these x-ray methods has led to a lack of detailed knowledge as to the conformation of the sugar-phosphate backbone in those forms of DNA that do not form diffractable crystals. A case in point is C-DNA, which forms under conditions of rather low relative humidity, in association with rather low concentrations of strongly binding metal ions such as Li^+, Mg^{+2}, and Na^+ (Rupprecht and Forslind, 1970; Arnott and Selsing, 1975). C-DNA is identified in x-ray fiber diffraction patterns as a distinct form with a 31-Å helix pitch and 9.33 basepairs per turn (Marvin et al., 1961). The base-stacking parameters may be used to build a structural model of C-DNA that is very similar to that of B-DNA (Marvin et al., 1961; Arnott and Selsing, 1975). Indeed, C-DNA is usually classified as a slightly distorted form of B-DNA.

Given the lack of experimental tools for examining this question, there have been few challenges to this view of C-DNA. One of the few independent studies, which did not rely on model building from the fiber diffraction constraints, used infrared linear dichroism of DNA fibers to evaluate the orientation of the phosphodiester groups (Pohle et al., 1984). These workers found a phosphodiester group orientation that is similar to that found in B-DNA, a conclusion to be challenged later in this paper.

A different approach for studying the molecular structure of DNA fibers is solid-state NMR (Alam and Drobny, 1991). For example, ^{31}P-NMR of oriented DNA fibers can reveal the orientation of the ^{31}P chemical shift tensors with respect to the helix axis because the orientation of the ^{31}P chemical shift anisotropy (CSA) tensors with respect to the phosphodiester linkage is known to a good approximation. This information is complementary to that obtained from

Received for publication 13 February 1997 and in final form 20 May 1997.

Address reprint requests to Dr. Malcolm H. Levitt, Division of Physical Chemistry, Arrhenius Laboratory, University of Stockholm, S-106 91 Stockholm, Sweden. Tel.: 46-8-162373; Fax: 46-8-152187; E-mail: mhl@physc.su.se.

Young K. Lee's current address is Quantum Magnetics, 740 Kenamar Court, San Diego, CA 92121.

S. C. Shekar's current address is Department of Molecular Biophysics and Biochemistry, Yale University, New Haven, CT 06520-8114.

0006-3495/97/09/1539/14 $2.00

x-ray diffraction studies, which are mainly sensitive to the base orientations.

Solid-state ^{31}P-NMR may be performed on both static and rotating samples. The earliest studies used static DNA fibers, with the samples mounted in a variety of directions with respect to the magnetic field. The orientation of the phosphodiester backbone was estimated for both A- and B-DNA samples (Nall et al., 1981; Shindo et al., 1985; Fujiwara and Shindo, 1985).

Greater sensitivity and resolution are achieved by employing a rotating sample instead of a static one. In magic-angle-spinning (MAS) NMR, the sample is rotated at a frequency of several kHz around an axis tilted by the "magic-angle," 54.74°, with respect to the static magnetic field. In the presence of strong rf fields at the Larmor frequency of the abundant protons ("proton decoupling"), the ^{31}P-NMR signal appears as a set of "rotational echoes." These echoes arise because the dispersed precessing magnetization vectors come back into phase every time the sample completes a full rotation. Fourier transformation of the signal yields a spectrum with sharp, intense spinning sidebands spaced at the spinning frequency for each nuclear site (Maricq and Waugh, 1979).

Harbison and Spiess derived a two-dimensional spectroscopic scheme involving synchronization of the radio-frequency pulse sequence with the sample rotation for investigating molecular orientations in partially ordered systems (Schmidt-Rohr and Spiess, 1994; Harbison and Spiess, 1986; Harbison et al., 1987; Blümich et al., 1987; Tang et al., 1989, 1990; Juang et al., 1995). In this sync-2D-MAS experiment, the ordered sample is loaded at a known angle relative to the rotor axis. The radio-frequency pulse sequence is synchronized with the sample rotation by using an optical signal reflected from the sample rotor. The delay between the synchronization time point and initiation of the pulse sequence is varied in a two-dimensional data acquisition scheme (Ernst et al., 1987). Orientational order of the sample is indicated by peaks in the 2D spectrum $S(\omega_1, \omega_2)$ at frequency coordinates $\omega_1 \neq 0$.

The amplitudes of the 2D spectral peaks may be analyzed to obtain the orientation distribution function (ODF) of ^{31}P CSA orientations with respect to the helix axis (Harbison et al., 1987; Schmidt-Rohr and Spiess, 1994). The ODF has peaks corresponding to the preferential ^{31}P CSA orientations. A particularly important feature of the NMR measurement is that it is not necessary to assume a single preferential orientation for the phosphodiester groups. An entire distribution function is obtained experimentally and, therefore, the presence of many different PO_4 orientations at the same time is readily detected. The results shown below clearly display resolution of at least three distinct phosphodiester bond orientations in the same sample.

The orientation distributions of CSA tensors can also be explored by a rotor synchronized two-dimensional phase-adjusted spinning sideband (PASS) pulse sequence (Song et al., 1996). This sync-2D-PASS method uses five radio-frequency π-pulses, in combination with a specific rotor synchronization scheme, to separate the sidebands associated with molecular order. Ideally, the sideband amplitudes and phases in sync-2D-PASS spectrum are identical to those provided by sync-2D-MAS, and may be analyzed in a similar fashion. The sync-2D-PASS method has the advantage of avoiding the overlap of spinning sideband manifolds, which is particularly important for systems containing many resolved chemical sites. In the present ^{31}P-NMR studies of oriented DNA, the advantages of sync-2D-PASS are not so pronounced, since only one ^{31}P spectral line is resolved. However, we still found sync-2D-PASS to be useful, especially when the peaks are inhomogeneously broadened, such as in the case of MgDNA. In the study described below, we used both methods more or less interchangeably.

Oriented DNA samples prepared by the wet-spinning method (Rupprecht, 1966, 1970; Rupprecht et al., 1991) are well suited for structural and dynamic investigations of high molecular weight DNA. Harbison and co-workers performed both ^{31}P and ^{13}C MAS investigations of oriented wet-spun DNA fibers (Tang et al., 1989, 1990; Juang et al., 1995). For the A and B forms of DNA, the orientation of the phosphodiester backbone was found to correspond well to the existing models of DNA conformation. It was also possible to demonstrate distortion of the phosphodiester backbone by the binding of an intercalating drug.

In the present study, we examine the influence of metal ion binding on the orientation of the phosphodiester groups. Of special interest is the orientation of the phosphate linkage in LiDNA and MgDNA samples identified as C-DNA by their x-ray fiber diffraction patterns. For these samples, we find a phosphate group ODF with two distinct peaks. The phosphate groups apparently adopt two distinct orientations. In one of these orientations, the O_3-P-O_4 planes are almost parallel with the helix axis, a situation that is very distinct from both A- and B-DNA. The second group of phosphates adopts an orientation that is similar, but not identical, to that of B-DNA.

In addition, we find evidence for considerable amounts of C-form DNA coexisting with the A-form in a sample of NaDNA. We also show results for DNA complexed with the minor groove binder netropsin. The ^{31}P ODF plots confirm that netropsin stabilizes the B-form of DNA.

MATERIALS AND METHODS

Sample preparation

Four kinds of oriented DNA samples were prepared with the wet spinning method (Rupprecht, 1966, 1970; Rupprecht et al., 1991), all with low salt contents: LiDNA and MgDNA from high molecular weight (1.17×10^7) calf-thymus NaDNA (Pharmacia Biotech Norden AB, Sollentuna, Sweden), and NaDNA and NaDNA-netropsin complex from high molecular weight salmon testes NaDNA (Fluka Chemie AG, Buchs, Switzerland). For the LiDNA sample, NaDNA was first dialyzed three times against 2 M LiCl, and then spun as LiDNA to achieve molecular orientation. The cylinder with spun deposit of LiDNA was finally bathed overnight in aqueous ethanol solution consisting of 80% ethanol + 0.02 M LiCl. All the other samples were spun as NaDNA. For the NaDNA sample, the cylinder with spun deposit was finally bathed in 75% ethanol + 0.03 M NaCl.

Oriented MgDNA was obtained by bathing a cylinder with spun deposit of NaDNA for four days in 75% ethanol solution containing 0.5 M $MgCl_2$, thereby exchanging the counterions (Rupprecht et al., 1991), and followed by bathing in 75% ethanol + 0.005 M $MgCl_2$. Research-grade netropsin hydrochloride ($C_{18}H_{26}N_{10}O_3 \cdot 2HCl$, see Fig. 1) was obtained from Serva Feinbiochemica (Heidelberg, Germany). The oriented NaDNA-netropsin complex was prepared by bathing a cylinder with spun deposit of NaDNA for one month in 75% ethanol solution containing 2 mM netropsin + 0.03 M NaCl. The netropsin input was ~0.36 drug/basepair, determined by measuring the optical density (at 300.9 nm) of the netropsin solution after bathing, then correlating with a pre-calibrated absorbance-concentration curve, assuming that the molecular weight was 662 per nucleotide basepair of NaDNA (Falk, 1966). In all cases, the spun deposits were finally slowly dried in a desiccator at +5°C whereby the fibers on the cylinder merged into a film of oriented material. After transfer of the desiccator to room temperature, the film was released from the cylinder, and equilibrated in an atmosphere of 75% relative humidity, as provided by saturated aqueous NaCl solution. The salt contents of the LiDNA and NaDNA samples were estimated as 0.6% LiCl and 1.3% NaCl, respectively, by weight of the dry sample (Rupprecht and Forslind, 1970). This corresponds to ~0.09 Li^+ and 0.14 Na^+ ions, respectively, per DNA basepair.

X-Ray diffraction

x-ray diffraction measurements were performed to check the crystallinity and conformations of the samples at 75% relative humidity. The oriented DNA films were folded into packs (~0.3 mm thickness) using a special folding apparatus, and mounted in a spring-loaded holder (Rupprecht and Forslind, 1970). A flat x-ray diffraction camera (Type PW 1030) with CuK_α radiation and a collimator of 500 μm was used to obtain the x-ray patterns. The specimen-to-film distance was 52.2 mm and the exposure time ~1 h. The x-ray diffraction patterns for the NaDNA-netropsin, NaDNA, LiDNA, and MgDNA samples are shown in Fig. 2. They display typical B-, A-, C-, C-type DNA diffraction patterns, respectively (Saenger, 1984).

Magic-Angle-Spinning ^{31}P-NMR

For magic-angle-spinning experiments, the 10-mm-wide oriented DNA films were folded into 10 × 1.8 × 1.8 mm^3 packs, which were slightly pressed to make the film layers stick together. The parallel-epipedic samples were stored in a desiccator at 75% relative humidity for a few days. Just before the NMR measurement, each sample was tightly covered with thin parafilm, then loaded into a standard Bruker double-bearing 4-mm ZrO_2 rotor with the fiber axis at 90° relative to the rotor axis. The remaining space was filled with Al_2O_3 powder to fix the DNA sample and to obtain good mechanical balance. The accurate orientation of the DNA fibers was verified by the almost vanishing spinning sideband amplitudes at odd multiples of the spinning frequency in the sync-2D-MAS experiments. A modified Bruker MSL 200 spectrometer (magnetic field B_0 = 4.7 T) was used, operating at a Larmor frequency $|\omega_0/2\pi|$ = 81.015 MHz for ^{31}P. The spinning speed was stabilized to ± 2 Hz by a home-built device.

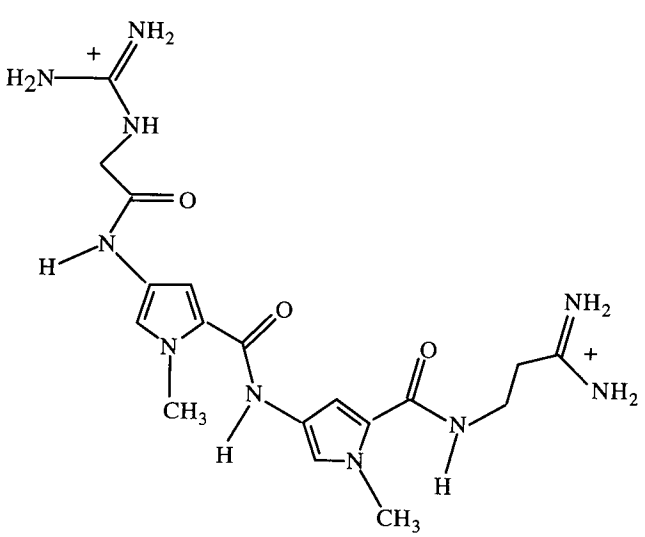

FIGURE 1 Molecular structure of netropsin.

The rotor-synchronized 2D-MAS pulse sequence is illustrated in Fig. 3. Rf fields at the ^{1}H Larmor frequency are denoted I, while rf fields at the ^{31}P Larmor frequency are denoted S. The position of the rotating sample holder is denoted schematically by the arrowed disks. The experiment starts when the rotor reaches a defined position indicated by the shaded symbol (in practice, this is defined by the position of the pen mark on the rotor). A "synchronization delay" τ_{sync} is inserted before a standard cross-polarization sequence (marked "CP") transfers polarization from the I-spins (^{1}H) to the S-spins (^{31}P).

Typically, we used a spinning frequency $|\omega_r/2\pi|$ = 2.000 kHz, a cross-polarization period of 2 ms, and acquired 243 transients with different pulse phases for each increment in the 2D signal acquisition scheme. Each signal transient lasted 17 ms. The ^{31}P rf field corresponded to a $\pi/2$ pulse duration of ~3 μs. For each sync-2D-MAS experiment, τ_{sync} was incremented in 16 steps between 0 and $\tau_r = |2\pi/\omega_r|$. Several experiments were also performed at the spinning frequencies of $|\omega_r/2\pi|$ = 1.600 and 1.400 kHz. The derived ODF's were reasonably consistent at all spinning frequencies. Only the results at 2.000 kHz are shown in this paper.

We also performed sync-2D-PASS experiments using the pulse sequence described in Song et al. (1996) with 256 t_1 increments. The results (not shown) also gave ODF's that were highly consistent with the sync-2D-MAS results. The consistency of experimental results over several days of consecutive measurements is evidence that the sample humidity was maintained sufficiently well for the purposes of this study.

Analysis of the results requires an estimate of the principal values of the ^{31}P CSA tensor. Independent one-dimensional magic-angle-spinning experiments were performed on randomly oriented NaDNA, LiDNA, MgDNA, and NaDNA-netropsin samples at the spinning frequencies $|\omega_r/2\pi|$ = 2.000, 1.700, 1.400, and 1.000 kHz. The spinning sideband amplitudes were analyzed using a newly developed fitting procedure (Antzutkin et al., unpublished observations) to derive the CSA $\sigma_{aniso} = \sigma_{zz} - \sigma_{iso}$ and the asymmetry parameter $\eta = (\sigma_{yy} - \sigma_{xx})/(\sigma_{zz} - \sigma_{iso})$, where $\sigma_{iso} = \frac{1}{3}(\sigma_{xx} + \sigma_{yy} + \sigma_{zz})$ and σ_{xx}, σ_{yy}, σ_{zz} are the CSA principal values. For each sample, the derived CSA and η values at different spinning frequencies were highly consistent. There was no evidence for spinning-induced sample orientation effects, as described in Gabriëlse et al. (1996). The estimated shielding anisotropy parameters (σ_{aniso}, η) and their standard deviations were as follows: (93.9 ± 0.7 ppm, 0.65 ± 0.03) for NaDNA-netropsin; (98.8 ± 0.7 ppm, 0.65 ± 0.03) for NaDNA; (92.5 ± 0.6 ppm, 0.64 ± 0.03) for LiDNA. The shielding parameters for MgDNA were more difficult to estimate because of the relatively broad peaks. We used the same values as for LiDNA, which were consistent with the MgDNA MAS data within experimental error. In the simulations, we used CSA values corresponding to the center of the relevant distributions, for example (93.9 ppm, 0.65) for NaDNA-netropsin. We checked that the results for the ODF were insensitive to the assumed CSA and η values within experimental error.

ANALYSIS OF THE 2D SPECTRA

The 2D spectra obtained by the sync-2D-MAS or sync-2D-PASS experiments were analyzed to obtain estimated orientation distribution functions (ODF's) of the ^{31}P CSA tensors with respect to the DNA helix axis. If the principal axis system of the ^{31}P CSA tensor is defined P, and a reference system with z-axis along the helix long axis is defined H, the ODF for the P ↔ H transformation is denoted

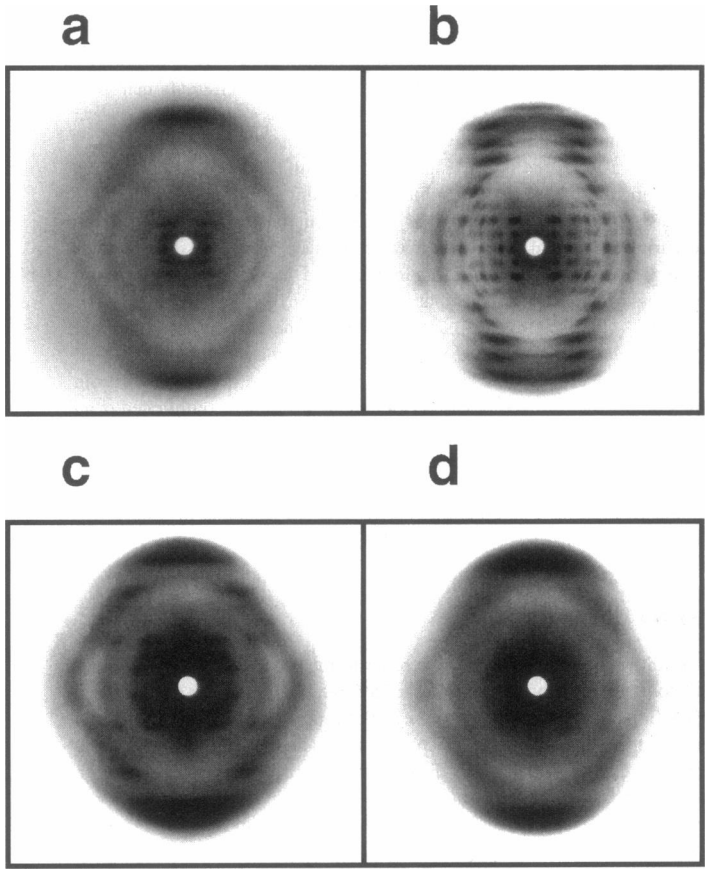

FIGURE 2 X-ray diffraction patterns of DNA fibers (low salt contents) at 75% relative humidity. (*a*) NaDNA-netropin; (*b*) NaDNA; (*c*) LiDNA; (*d*) MgDNA.

$P(\Omega_{PH})$, where Ω_{PH} indicates the three Euler angles $\Omega_{PH} = (\alpha_{PH}, \beta_{PH}, \gamma_{PH})$. These Euler angles are defined as in Varshalovich et al. (1988). The principal axis system P is brought into coincidence with the helix axis system H by the following series of rotations: 1) a rotation around the z axis of the system P through the angle α_{PH}; 2) a rotation around the "new" y axis through the angle β_{PH}; and 3) a rotation around the z axis of the system H through the angle γ_{PH}. The angle β_{PH} is subtended by the z axes of P and H.

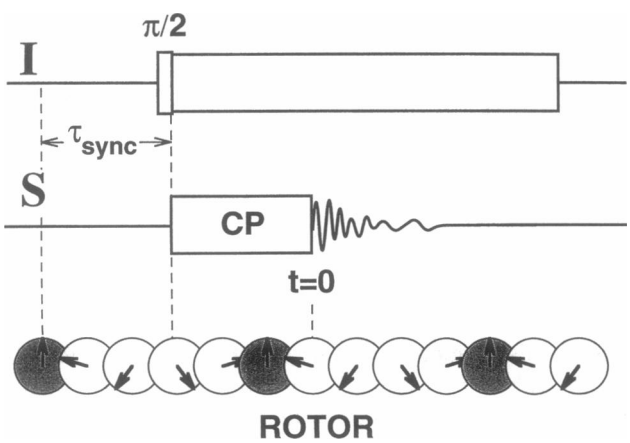

FIGURE 3 Sync-2D-MAS pulse sequence.

The distribution function of $P(\Omega_{PH})$ is the joint probability distribution of the three random variables α_{PH}, cos β_{PH}, and γ_{PH}: $P(\Omega_{PH}) = P(\alpha_{PH}, \cos \beta_{PH}, \gamma_{PH})$. Peaks in the probability distribution reflect preferential orientations of ^{31}P CSA tensors with respect to the DNA helix. If an assumption is made as to the local CSA orientation with respect to the phosphodiester linkage (see below), this ODF reflects directly the orientations of the phosphodiester groups with respect to the helix, and provides strong structural constraints on the geometry of the phosphodiester-sugar backbone.

The details of our analysis method will be presented fully elsewhere (Levitt, unpublished observations). In large part, the analysis follows that of Harbison et al. (1987), but there are some differences, which are indicated briefly below.

Following Harbison et al. (1987), we write an expression of the P ↔ H ODF in terms of orthogonal Wigner functions:

$$P(\Omega_{PH}) = \sum_{L=0}^{L_{max}} \sum_{q,q'=-L}^{L} P^{PH}_{Lqq'} D^{L}_{qq'}(\Omega_{PH}) \qquad (1)$$

where the ODF components $P^{PH}_{Lqq'}$ are assumed to be negligible above a certain rank $L > L_{max}$. The ODF is determined by estimating a limited number of spherical components $P^{PH}_{Lqq'}$, which are complex numbers in general.

The distribution function $P(\Omega_{PH})$ is not directly accessible by experiment. The directly accessible distribution function is $P(\Omega_{PD})$, which applies to the transformation from the CSA principal axis frame to a director frame D with z axis along the fiber axis. The orientations of the DNA molecules with respect to the fiber axis are governed by a further distribution $P(\Omega_{HD})$. If the $P(\Omega_{PH})$ and $P(\Omega_{HD})$ distributions are statistically independent, the following chain rule for the spherical components applies (Levitt, unpublished observations):

$$P^{PD}_{Lqq'} = \frac{8\pi^2}{2L+1} \sum_{q''} P^{PH}_{Lqq''} P^{HD}_{Lq''q'} \quad (2)$$

To simplify the analysis, we assume that the moments of the H ↔ D transformation are

$$P^{HD}_{Lq''q'} = \begin{cases} P^{HD}_{L00}\delta_{q''0}\delta_{q'0} & \text{for L even} \\ 0 & \text{for L odd} \end{cases} \quad (3)$$

This corresponds to perfectly uniaxially oriented fibers, with no preferential direction for the double helix winding axis. In practice, static ^{31}P- and ^{2}H-NMR indicate a spread in β PD of up to $\pm 10°$ (Brandes et al., 1988a,b; Nall et al., 1981), so our final ODF is also expected to have an accuracy of up to $\pm 10°$.

The above property of H ↔ D transformation limits our knowledge of the structurally significant P ↔ H transformation. In particular, the γ_{PH} part of the distribution is inaccessible to experiment, and only components of even rank L may be derived. Additional symmetries in the spin interactions further restrict the amount of accessible information. As shown elsewhere (Levitt, unpublished observations), only the real parts of the moments P^{PH}_{Lq0} (L and q even) are experimentally accessible. Hence a peak in the determined $P(\alpha_{PH}, \cos\beta_{PH})$ distribution at angles $(\alpha_{PH}, \beta_{PH})$ may in fact be due to 8 possible distinct orientations of the ^{31}P CSA tensor: $(\pm\alpha_{PH}, \beta_{PH})$, $(\pi \pm \alpha_{PH}, \beta_{PH})$, $(\pm \alpha_{PH}, \pi - \beta_{PH})$ and $(\pi \pm \alpha_{PH}, \pi - \beta_{PH})$. This ambiguity should be borne in mind when basing structural models on the results shown below.

Following Harbison et al. (1987), the numbers $\mathrm{Re}\{P^{PH}_{Lq0}\}$ are determined from the best fit to the equation

$$a^{k_1k_2} \cong \sum_{L=0,2,\ldots}^{L_{max}} \sum_{q=0,2,\ldots}^{L} a^{k_1k_2}_{Lq0} Re\{P^{PH}_{Lq0}\} \quad (4)$$

where $a^{k_1k_2}$ are experimental sideband amplitudes derived by either sync-2D-MAS or sync-2D-PASS, and $a^{k_1k_2}_{Lq0}$ are "subspectral sideband amplitudes," derived by numerical computation. The indices k_1 and k_2 are the sideband coordinates in the 2D spectrum in units of the spinning frequency. In all cases, we integrated the entire spectral sidebands, ignoring inhomogeneous amplitude distributions, which sometimes give rise to a dispersion-like appearance.

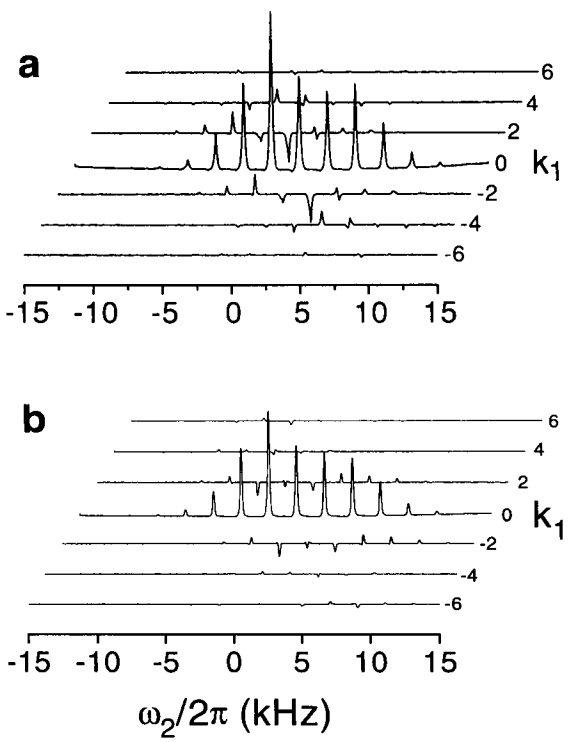

FIGURE 4 Sync-2D-MAS ^{31}P spectra of oriented DNA fibers, obtained at 75% relative humidity, 2000 Hz spinning frequency, and with the fiber axis oriented at $\pi/2$ relative to the rotor axis. (*a*) NaDNA-netropsin; (*b*) NaDNA.

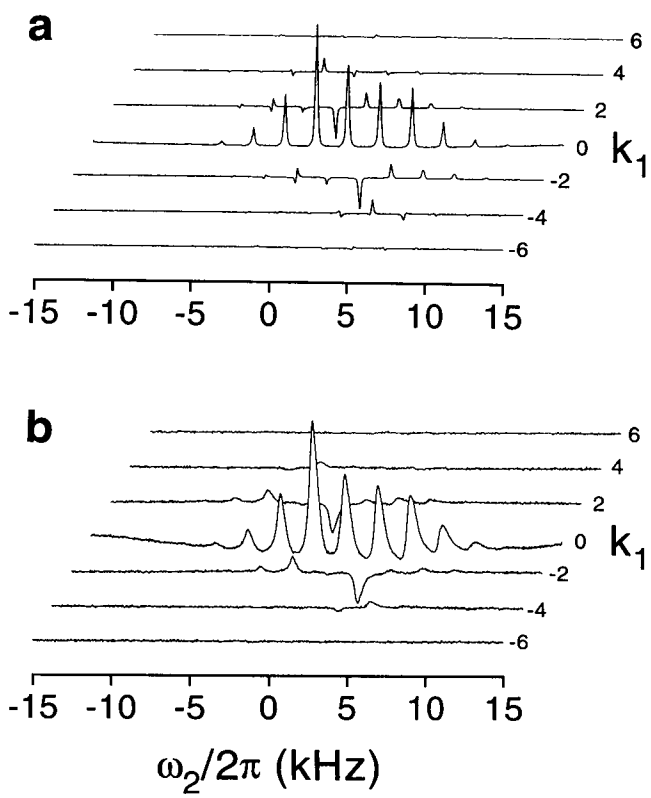

FIGURE 5 Sync-2D-MAS ^{31}P spectra of oriented DNA fibers, obtained under the same conditions as in Fig. 4. (*a*) LiDNA; (*b*) MgDNA.

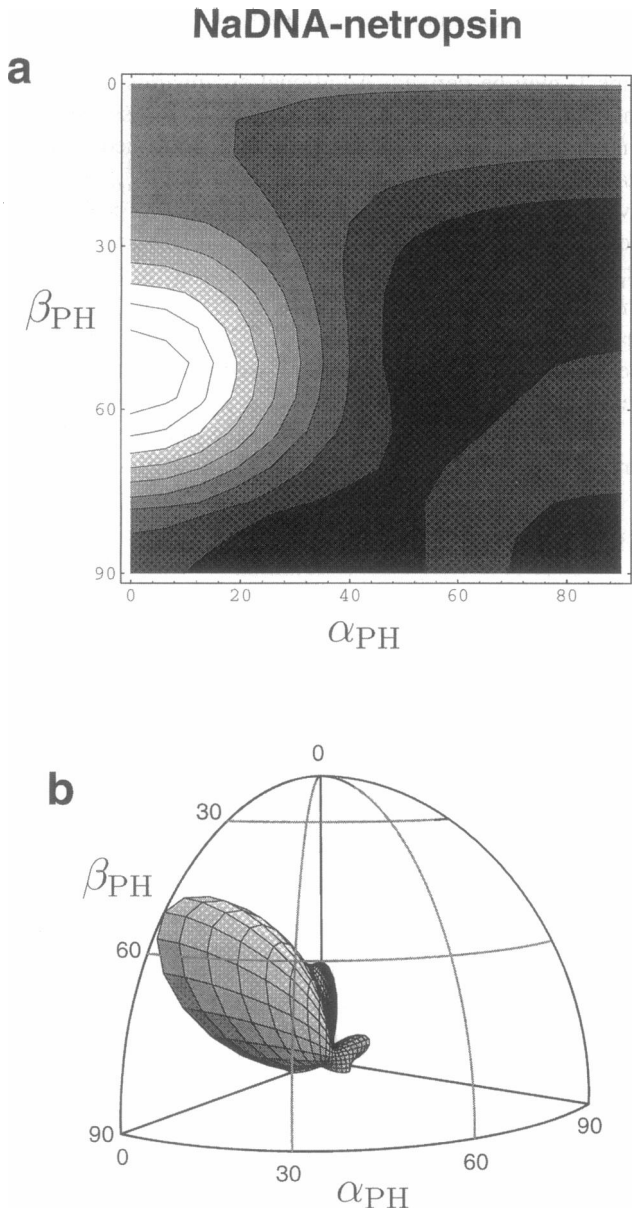

FIGURE 6 ODF of the ^{31}P CSA tensors with respect to the DNA helix axis in NaDNA-netropsin fibers. (*a*) Contour plot; (*b*) polar surface plot.

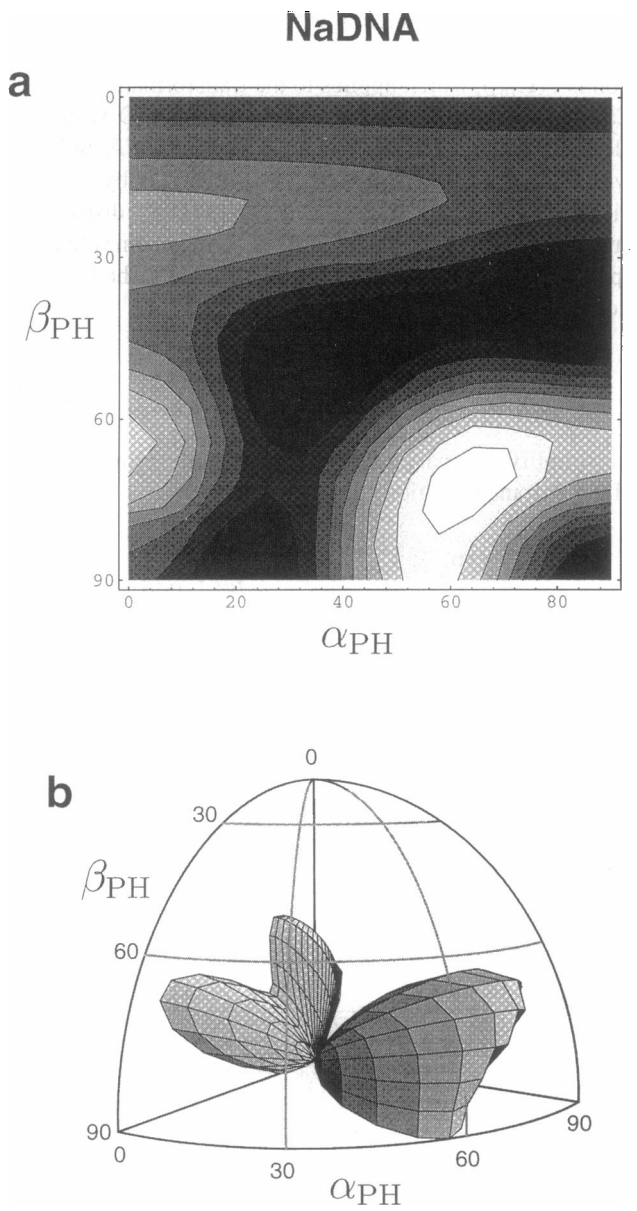

FIGURE 7 ODF of the ^{31}P CSA tensors with respect to the DNA helix axis in NaDNA fibers. (*a*) Contour plot; (*b*) polar surface plot.

In addition, we implemented a new algorithm for simulation of the subspectral amplitudes $a_{Lq0}^{k_1k_2}$. Harbison et al. (1987) evaluated these amplitudes by a three-dimensional integration over three angles, which is very time-consuming and potentially inaccurate for high rank L. We used identities from angular momentum group theory to reduce these amplitudes to combinations of two-dimensional integrals, which may be evaluated faster and more accurately. We believe that the improved simulation procedure, which allows accurate evaluation of $a_{Lq0}^{k_1k_2}$ out to ranks L~12, is one of the factors leading to the high quality of our derived distribution functions. Details will be published elsewhere (Levitt, unpublished observations).

A further innovation is that we do not derive the best fit to Eq. 4 by direct inversion of the linear system of the equations, as recommended by Schmidt-Rohr and Spiess (1994). In practice, we found that this "direct" method easily over-interprets the experimental data, giving rise to physically unreasonable probability distributions that are negative in some regions of orientational space. Instead, we used an iterative search method for the best fit, gradually introducing more ranks L until the fit no longer improves significantly, all the time penalizing negative probabilities. The results of this nonlinear fit are always physically reasonable, and we usually attain a final fit to the experimental amplitudes that is as good as with the direct method, within experimental errors.

One final problem should also be mentioned. As pointed out by Schmidt-Rohr and Spiess (1994), the signs of the

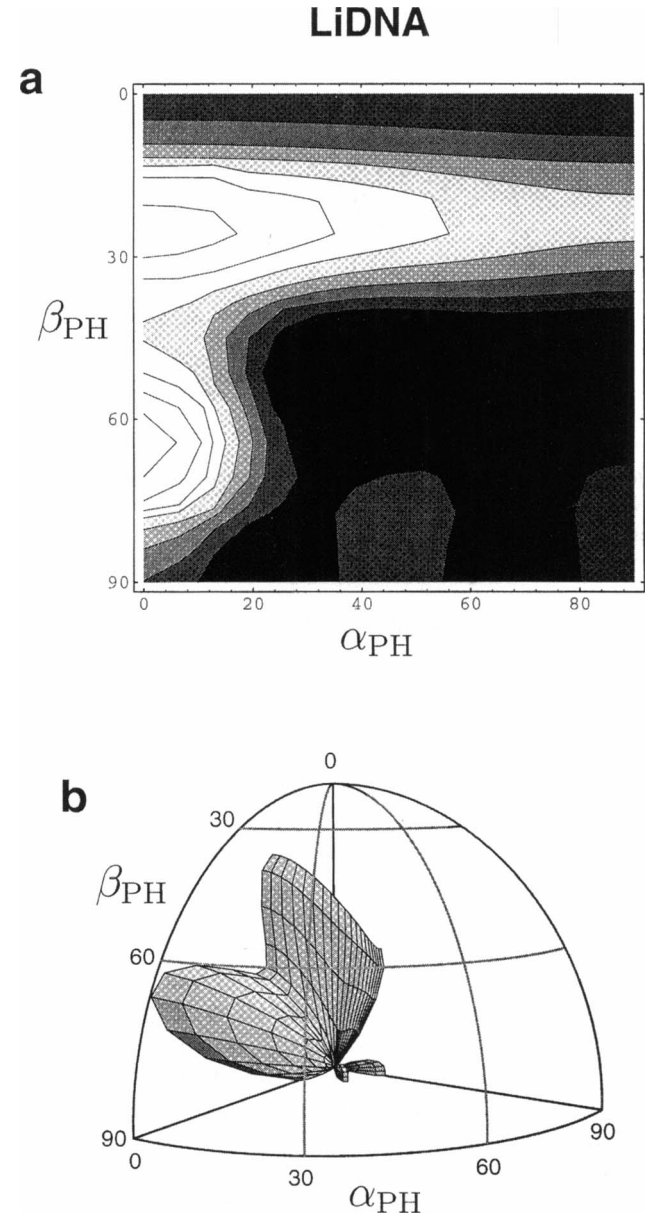

FIGURE 8 ODF of the ^{31}P CSA tensors with respect to the DNA helix axis in LiDNA fibers. (*a*) Contour plot; (*b*) polar surface plot.

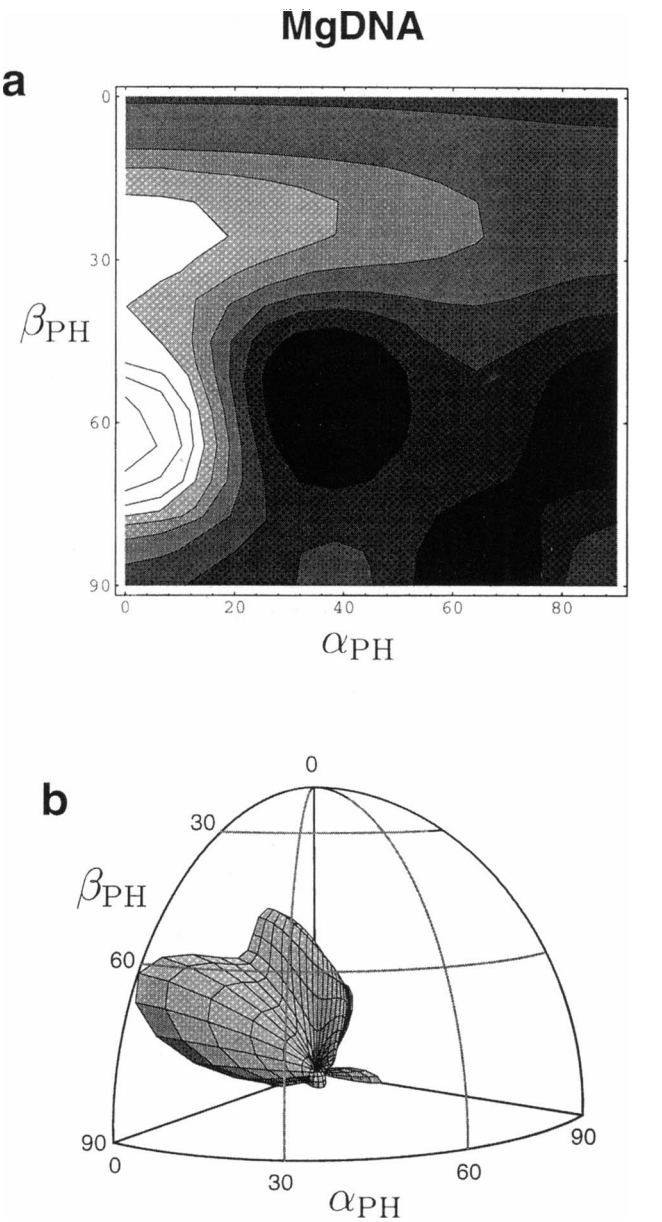

FIGURE 9 ODF of the ^{31}P CSA tensors with respect to the DNA helix axis in MgDNA fibers. (*a*) Contour plot; (*b*) polar surface plot.

experimental amplitudes $a^{k_1k_2}$ cannot be determined unambiguously. If the orientation of the fiber in the rotor with respect to the optical synchronization system is unknown, each set of experimental results has two possible interpretations, related by sign inversion of peaks with even index k_1 in the 2D spectra. Typically, these two interpretations give very different orientation distribution functions. In practice, we simply performed the analysis twice, using two distinct sign interpretations, and rejected orientation distribution functions that were obviously unreasonable. In all cases we examined, the correct choice was clear. This ambiguity might be resolved in the future by determining the orientation of the fiber in the rotor independently.

The above procedure leads to a distribution function $p(\alpha_{PH}, \cos \beta_{PH})$ for the orientation of the ^{31}P CSA tensors with respect to the helix, bearing in mind the ambiguity in α_{PH}, and β_{PH}, as mentioned above. In the results section, these distribution functions are represented in two ways: 1) as contour plots, with light regions denoting high probability and dark regions representing low probability; and 2) as polar surface plots, in which the radius from the origin is proportional to the probability density (the enclosed volume of the plotted surface is equal to one). The contour plots give a more accurate estimation of coordinates, while the polar surface plots are more visually accessible.

Interpretation of these results in terms of the molecular structure of DNA requires additional assumptions as to the

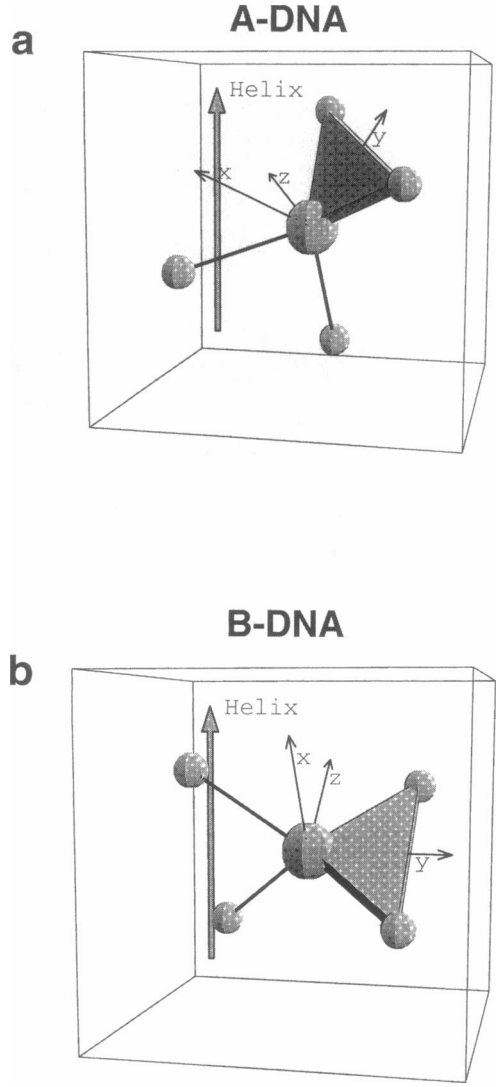

FIGURE 10 View of the predominant phosphate orientations, deduced from Figs. 6 and 7. (*a*) A-DNA; (*b*) B-DNA. The attached axis system (*x*, *y*, *z*) corresponds to the assumed orientations of the ^{31}P CSA principal axes.

local orientation of the ^{31}P CSA with respect to the phosphodiester linkage. Herzfeld et al. (1978) used a single crystal of barium diethyl phosphate (BDEP) as a model compound to investigate the "standard orientations" of ^{31}P shielding tensors in the phosphodiester linkage. The principal axis of the ^{31}P shielding tensors in BDEP was found to be ~10° away from the local molecular symmetry axes of the approximately tetrahedral phosphate group, with 1) the least-shielded $\vec{x}^P$ axis approximately perpendicular to the O_3-P-O_4 plane formed by the phosphorus and the two unsubstituted oxygens; 2) the intermediate-shielded $\vec{y}^P$ axis near the bisector of the O_3-P-O_4 bonds on the plane; and 3) the most-shielded $\vec{z}^P$ axis perpendicular to $\vec{x}^P$ and $\vec{y}^P$.

In the following discussion, it is assumed that in DNA the principal axes of the ^{31}P CSA tensors have the same relationship to the local PO_4 group symmetry axes within ~20° deviation. This assumption seems reasonable in view of the

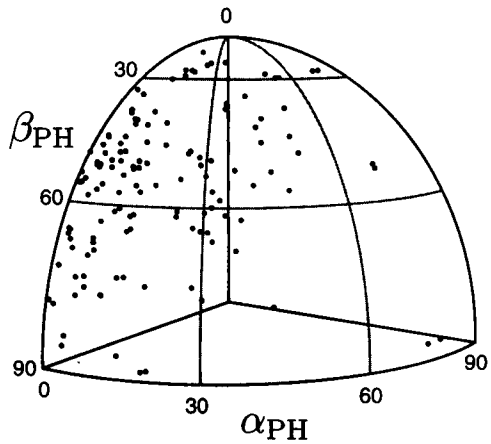

FIGURE 11 Polar scatter plot of the Euler angles of the phosphates in six oligonucleotide-netropsin complexes. Each set of Euler angles is represented as a dot lying on the spherical surface.

fact that the principal values of the ^{31}P CSA tensors are very similar in DNA and BDEP, and do not change very much between different forms of DNA. The assumption is also supported by the fact that at least for A- and B-DNA, both Harbison and co-workers (Tang et al., 1989, 1990; Juang et al., 1995) and ourselves derived PO_4 orientations in good agreement with independent methods.

In one case, we also show ^{31}P orientation distributions derived from x-ray crystallography of oligonucleotides. For each crystal structure, the orientations of the local symmetry axes of the PO_4 groups were derived from the atomic coordinates. The helix axis was determined fairly crudely by determining the inertial tensor and using the principal axis associated with the smallest eigenvalue. The principal axes of the chemical shift tensors were attached to the PO_4 groups using the local orientations given above. This allowed Euler angles Ω_{PH} to be estimated for the 20–24 PO_4 groups in each crystal structure. The plotted angle along the α_{PH} axis is actually $\pi - \text{mod}(\alpha_{PH}, \pi)$ in the case of $\text{mod}(\alpha_{PH}, \pi) > \pi/2$, and $\text{mod}(\alpha_{PH}, \pi)$ otherwise. The same applies to β_{PH}. This manipulation matches the ambiguity in the Euler angle distribution derived from the NMR results (see above). The crystal Euler angles display considerable scatter. In part this is because of the rather crude determination of the helix axis, but the main causes of the scatter are probably end effects in these small molecules and distortions caused by crystal packing (Chandrasekaran and Arnott, 1996). Typically, the experimentally determined PO_4 orientations in the DNA fibers are much more sharply defined than those observed in oligonucleotide crystals.

RESULTS AND DISCUSSION

2D-MAS spectra

Figs. 4 and 5 show 2D-MAS spectrum for NaDNA-netropsin, NaDNA, LiDNA, and MgDNA, all at 75% relative humidity, and obtained at a spinning frequency of 2000 Hz.

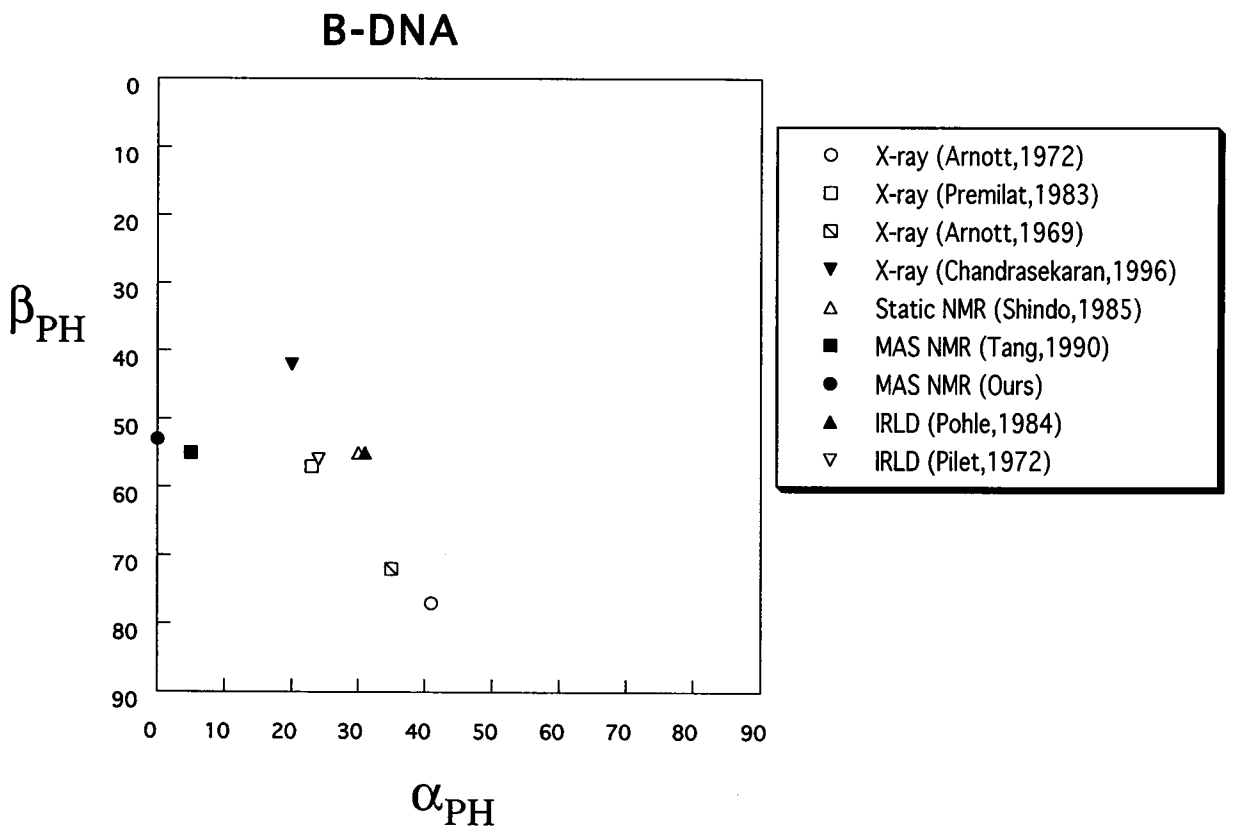

FIGURE 12 Estimated phosphate group orientations in B-DNA fibers, obtained by various methods. All methods have an error margin of ~10–20°.

The spectra show spinning sidebands along the horizontal axis, and resolution of sidebands representing the molecular order along the vertical axis, indexed by the integer k_1. Only even-numbered slices are shown. The odd slices contain almost no signal since the samples were mounted such that the angle between the fiber axis and rotor axis was $\pi/2$.

Most of the spectra have a rather similar appearance, although examination shows that the spinning sideband amplitudes are quite variable. An exception is the MgDNA spectrum (Fig. 5 *b*), which has much broader peaks. It was verified by spin echo experiments that the major source of broadening in MgDNA is inhomogeneous. This is possibly due to local interactions of the divalent Mg^{+2} ions with the phosphate groups, leading to a heterogeneity in the isotropic ^{31}P chemical shifts. The sync-2D-PASS method was particularly useful in this case for resolving the partially overlapping spinning sideband patterns (spectra not shown).

^{31}P CSA orientation distribution functions

Figs. 6-9 show the ODF's of the ^{31}P CSA tensors with respect to the helix axis, derived from sync-2D-MAS spectra, for the NaDNA-netropsin, NaDNA, LiDNA, and MgDNA samples, respectively. The dark areas in the contour plots correspond to lower orientation probabilities, while the light areas show the most probable orientations. The polar surface plots have the advantage of removing the distortions associated with projecting the spherical orientational space onto a plane.

NaDNA-netropsin

The ^{31}P ODF for NaDNA-netropsin (Fig. 6) displays, to a good approximation, a single strong orientational peak centered at $(\alpha_{PH}, \beta_{PH}) \cong (0°, 53°)$. This is in good agreement with earlier sync-2D-MAS studies (Tang et al., 1990; Juang et al., 1995), who obtained maximum probability ($\alpha_{PH} = 5°$, $\beta_{PH} = 55°$) for pure B-form LiDNA and a similar result for the groove-binding daunomycin-DNA complex. As discussed below, this strong peak corresponds to the orientation of the phosphodiester linkage in the B form of DNA. Netropsin is known to stabilize the B form by binding to the minor groove (Wartell et al., 1974; Flanagan et al., 1995; Kopka et al., 1985a,b; Rhee et al., 1993; Patel and Shapiro, 1985; Coll et al., 1989). The binding of netropsin causes a partial or total suppression of the B → A conformational transition at low relative humidity (Fritzsche, 1994; Fritzsche et al., 1984a,b, 1992; Pohle and Fritzsche, 1984). Each bound netropsin molecule spans ~4–5 A-T basepairs, but its effect to stabilize B-DNA may extend to ~24 basepairs along the helix. The suppression of the B → A transition is complete when the netropsin input in NaDNA fibers is ~0.1 drug/basepair (Fritzsche et al., 1984a). Since our sample was prepared with 0.36 drug/basepair, there was

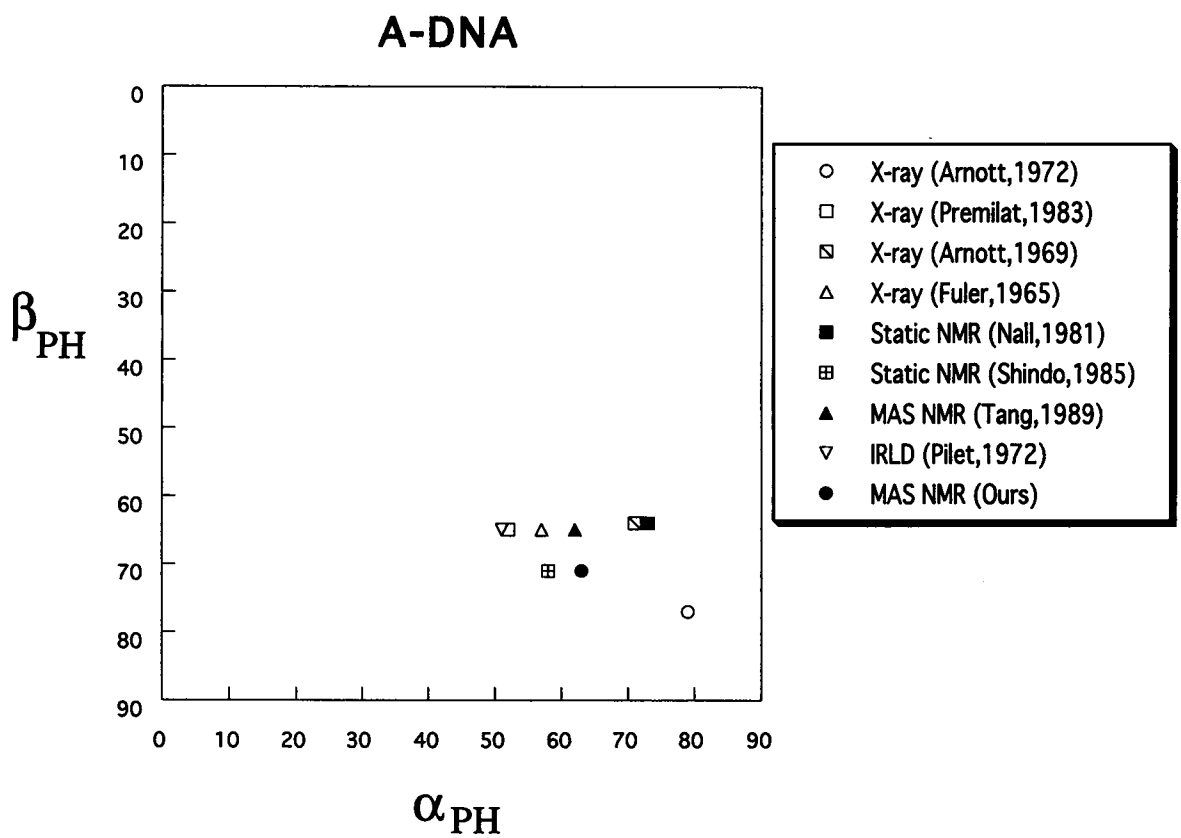

FIGURE 13 Estimated phosphate group orientations in A-DNA fibers, obtained by various methods. All methods have an error margin of ~10–20°.

more than enough netropsin present to maintain B-DNA. Indeed, the x-ray diffraction displayed a typical B form pattern (Fig. 2 *a*).

NaDNA

The ODF for NaDNA in the absence of netropsin is much more complex (Fig. 7). Three strong peaks appear. The major feature is a broad ridge at a CSA orientation of (α_{PH}, β_{PH}) ≅ (63°, 71°). We assign this peak to the A form of DNA, with the support of the x-ray diffraction pattern (Fig. 2 *b*). The location of this peak agrees again with previous determinations (Tang et al., 1989). Under the conditions used, however, not all of the DNA is in the A form. The two subsidiary peaks correspond to a significant fraction of DNA molecules in different conformations. Experiments on different samples gave results with varying proportions of these three peaks. Under no conditions, however, was a pure A-form ODF observed. We discuss the two additional peaks in the ODF for NaDNA below.

LiDNA

The ODF for LiDNA is shown in Fig. 8. This displays two peaks, which coincide with the subsidiary features observed in the NaDNA ODF. The main peak is at the orientational coordinates (α_{PH}, βPH) ≅ (0°, 65°), while the minor peak is at (α_{PH}, βPH) ≅ (0°, 25°). The major peak is in a position close, but not identical to, the peak for NaDNA-netropsin assigned to B-DNA.

One possible interpretation of the LiDNA ODF is that the DNA is predominantly in the B form, with an extra component, possibly the C form. One argument against this interpretation is that the main ODF peak in LiDNA is not at exactly the same position as that expected of B-DNA. This discrepancy was observed in a wide range of samples. In addition, the x-ray diffraction pattern of LiDNA does not obviously show the superposition of two forms. Instead, a typical C-form pattern is displayed. It was established earlier that wet-spun LiDNA prepared at low LiCl content occurs in the C form (Rupprecht and Forslind, 1970).

Another possible interpretation of the LiDNA ODF is that the DNA is in an essentially pure C form, but the C form itself incorporates phosphodiester linkages with two different orientations. It should be recalled that Z-DNA, which forms in certain nucleotide sequences under higher salt concentrations, also displays two distinct phosphodiester orientations.

These two interpretations may be distinguished by performing ^{31}P-^{31}P spin diffusion experiments, which are planned.

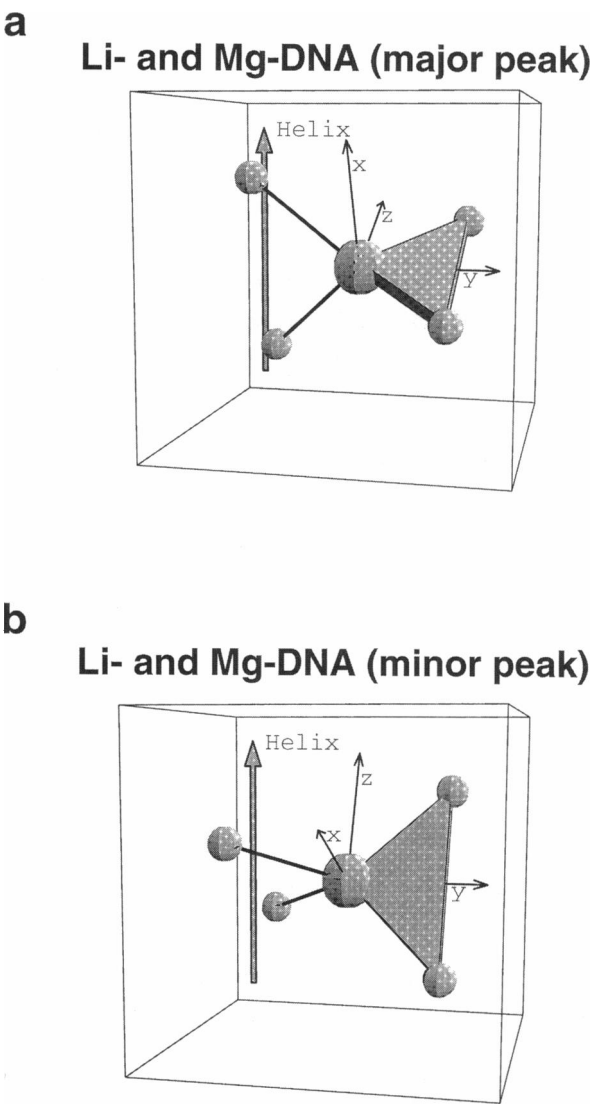

FIGURE 14 View of the predominant phosphate orientations in LiDNA and MgDNA, deduced from Figs. 8 and 9. (*a*) Major ODF peak; (*b*) minor ODF peak.

MgDNA

The ODF for MgDNA (Fig. 9) is very similar to that of LiDNA (Fig. 8). The spectral broadening in MgDNA does not seem to be associated with much of a change in the phosphate group orientations. The two peaks in the ODF are in the same position as for LiDNA. However, the minor peak appears to be smaller than in LiDNA. X-ray diffraction shows a typical C-type pattern (Fig. 2 *d*).

It is interesting to note that the minor component of the ODF in NaDNA (Fig. 7) has precisely the same form as the ODF for LiDNA (Fig. 8). The NaDNA result may therefore be attributed either to a coexistence of all 3 forms (A, B, and C), or of two forms (A and C), with the C form displaying two conformations. On the other hand, the ODF plots of LiDNA and MgDNA do not show the existence of an A-form peak. This is in accordance with previous observations that LiDNA and MgDNA never adopt the A form (Schultz et al., 1994; Rupprecht et al., 1994).

Phosphate group orientations

By assuming that the orientations of the ^{31}P shielding tensor principal axes have the same relationship to the phosphodiester linkage as in barium diethyl phosphate, it is possible to deduce the orientation of the PO_4 group with respect to the helix in the different conformational forms of DNA. The accuracy of this estimation is expected to be $\sim\pm 20°$.

The deduced phosphodiester orientations for the major components in NaDNA and NaDNA-netropsin are shown in Fig. 10, *a* and *b*. In these diagrams, the O_3-P-O_4 plane, where O_3 and O_4 are the non-bonded oxygens, is depicted as a wedge. The assumed principal axis system of the ^{31}P shielding tensors is also shown on the plots as *x*, *y*, *z*.

As discussed above, we attribute the preferential orientations in Fig. 10, *a* and *b* to the A and B form of DNA, respectively. The phosphate group orientations in these systems are very different. It should be noted that the larger α_{PH} angle in A-DNA contracts the distance spanned by the ester oxygens along the helix. This is in accordance with the fact that the residue translation is 2.56 Å for A-DNA, but 3.38 Å for B-DNA (Saenger, 1984).

The experimental NaDNA-netropsin ODF was compared with phosphate group orientations in crystalline oligonucleotide-netropsin complexes. Fig. 11 shows a scatter plot of ^{31}P CSA orientations obtained from the crystal structures of six oligonucleotides complexed with netropsin (Coll et al., 1989; Kopka et al., 1985b; Tabernero et al., 1993; Balendiran et al., 1995; Goodsell et al., 1995). The qualitative agreement with Fig. 6 *b* is gratifying.

The phosphate group orientations obtained by a variety of different methods are compared graphically for B-DNA in Fig. 12, and for A-DNA in Fig. 13. These plots show the Euler angles relating a local axis system P attached to the phosphate group to a frame H with the *z* axis along the helix. The local axis system P is attached to the PO_4 group, as shown in Figs. 10 and 14. This is the same orientation as that assumed for the ^{31}P CSA tensor in the NMR experiments.

The agreement is rather good for B-DNA and very good for A-DNA. For B-DNA, the NMR results tend toward a Euler angle α_{PH} which is $\sim$20–30° smaller than that derived from other methods. It is possible that this reflects a small rotation of the CSA principal axis system in B-DNA with respect to BDEP. Another contributing factor is the tendency for the NMR-derived ODF to be "attracted" to the $\alpha_{PH} = 0$ axis, by merging with its mirror image in the $\alpha_{PH} = 0$ axis, as discussed by Schmidt-Rohr and Spiess (1994). On the other hand, the angles estimated from x-ray structures of oligonucleotides complexed with netropsin (Fig. 11 *a*) do seem to cluster around the NMR-determined orientation, which adds support to the validity of the NMR results. It should be recalled that x-ray fiber diffraction provides no

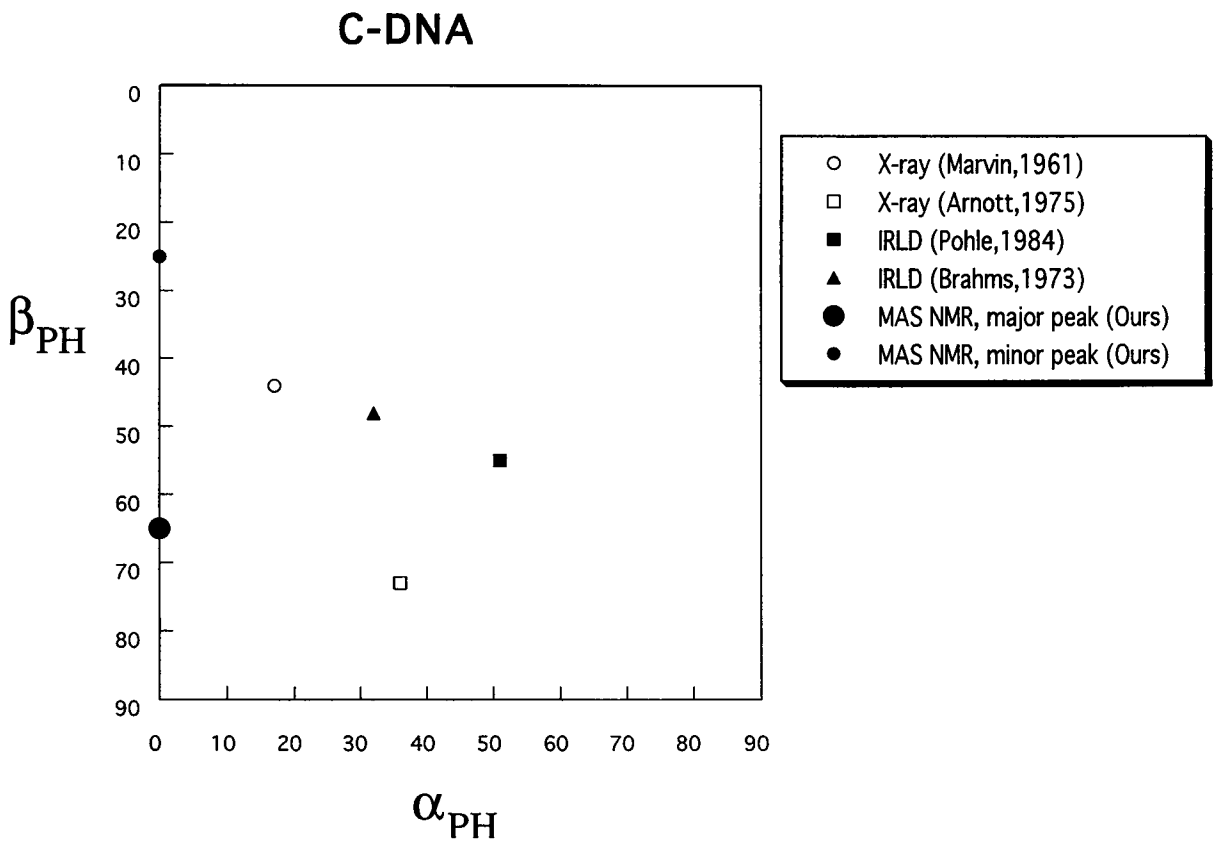

FIGURE 15 Estimated phosphate group orientations in C-DNA fibers, obtained by various methods. All methods have an error margin of ~10–20°.

direct information as to the PO_4 group orientations—these have to be deduced by model building and refinement with the constraints of the basepair geometry. Infrared dichroism, on the other hand, does observe the phosphate groups directly, but, like NMR, requires assumptions as to the orientations of the transition moments with respect to the local molecules group.

The estimated phosphate group orientations for the major and minor peaks of LiDNA and MgDNA are shown in Fig. 14. The major orientational component is similar to that of B-DNA, but with the O_3-P-O_4 planes rotated slightly about their bisector so as to become more perpendicular to the helix axis. The minor orientational component is rotated in the opposite direction, so as to produce O_3-P-O_4 planes that are almost parallel to the helix axis. This rotation leads to the contraction of the distance spanned by the ester oxygens along the helix. This is consistent with the shorter pitch of C-DNA compared to B-DNA.

In order to elucidate C-DNA structure, it will be necessary to establish whether the LiDNA and MgDNA samples contain a mixture of DNA conformations, or whether C-DNA itself supports two different phosphate group orientations.

For C-DNA, there have been few previous structural studies. The only independent determination of PO_4 group orientations is by infrared linear dichroism of the PO_2 vibrations (Pohle et al., 1984). That result is quite different (see Fig. 15 and Table 1). The present NMR result also disagrees sharply with the estimate from model building based on x-ray diffraction constraints (Marvin et al., 1961; Arnott and Selsing, 1975), which agrees roughly with the IR data. The IRLD and x-ray diffraction-based model orientations resemble much more closely the PO_4 orientations in A-DNA. However, it should be recalled that the analysis of the IRLD and x-ray diffraction results assumed a uniform DNA structure.

At the moment, the discrepancy between these estimates is not understood. We consider our estimate of PO_4 orientations to be unequivocal and clearly inconsistent with previous models, well outside the bounds of the experimental error. The discrepancy is too large to be plausibly explained by a shift in the ^{31}P CSA principal axes.

A summary of phosphodiester group orientations in C-DNA samples, estimated by different methods, is shown in Table 1.

In conclusion, rotor synchronized 2D-MAS and 2D-PASS methods may be used to characterize the orientation of the phosphodiester backbone in A-, B- and C-DNA. The NaDNA-netropsin complex displays a single phosphate orientation attributed to the pure B form. The LiDNA and MgDNA samples display two phosphate group orientations, which could be interpreted either as a mixture of a slightly distorted B form and a C form, or as a pure C form alone, if that form itself supports two phosphate conformations.

TABLE 1 The Euler angles of the phosphodiester groups in A-, B-, and C-DNA fibers, obtained from different methods

Method	A-DNA		B-DNA		C-DNA		Ref.
	α_{PH}	β_{PH}	α_{PH}	β_{PH}	α_{PH}	β_{PH}	
MAS NMR*	65	72	0	53	{0 {0	{65 {25	This article
	62	65	5	55			Tang et al., 1989, 1990
Static NMR	58 73	71 64	30	55			Shindo et al., 1985 Nall et al., 1981
X-ray#	−79	77	−41	77	−36	73	Arnott and Selsing, 1975; Arnott and Hukins, 1972
	−71	64	−35	72			Arnott et al., 1969
	52	65	23	57			Premilat and Albiser, 1983
	−61	61	20	42			Chandrasekaran et al., 1989; 1996
	−57	65			−17	44	Marvin et al., 1961; Fuller et al., 1965
IRLD§			31	55	35	50	Pohle et al., 1984
	51	65	24	56	32	48	Pilet and Brahms, 1972; Brahms et al., 1973

The Euler angles refer to the relationship between a local system P attached to the phosphodiester group, and a helix axis system H with z axis along the helix long axis. The orientation of P with respect to the phosphodiester groups is shown in Fig. 10. This coincides with the expected principal axis orientation of the ^{31}P CSA tensors in NMR measurements.

*The angles for the P ↔ H transformation are determined directly.

#The angles are determined from the estimated PO_4 group coordinates by attaching an axis system P as illustrated in Fig. 10.

§Estimated from the orientation of the transition moments of the antisymmetric and symmetric stretching vibrations of PO_2 at 1230 cm^{-1} and 1090 cm^{-1}, respectively, relative to the DNA helix axis.

The NaDNA sample equilibrated at 75% relative humidity is predominantly in the A form, but there are considerable minor components with a similar distribution of phosphate orientations to that found in LiDNA. The orientations of the ^{31}P chemical shift tensors with respect to the DNA helix axis in A- and B-DNA are in good agreement with those obtained from other methods. The orientation of the phosphate linkage in C-DNA is in conflict with previous results deduced from infrared linear dichroism and x-ray fiber diffraction. Current concepts of C-DNA structure may have to be revised.

We thank T. Karlsson and O. G. Johannessen for implementation of the spinning-speed controller and sustained help. We thank G. S. Harbison, B. Nordén, L. Kadalayil, and H. Fritzsche for discussions and comments.

This work was supported by the Swedish Natural Science Research Council and the Swedish Medical Research Council.

REFERENCES

Alam, T. M., and G. P. Drobny. 1991. Solid-state NMR studies of DNA structure and dynamics. *Chem. Rev.* 91:1545–1590.

Arnott, S. 1980. Twenty years hard labor as a fiber diffractionist. *Fiber Diffr. Methods, ACS Symp. Ser.* 141:1–30.

Arnott, S., S. D. Dover, and A. J. Wonacott. 1969. Least-squares refinement of the crystal and molecular structures of DNA and RNA from x-ray data standard bond lengths and angles. *Acta Crystallogr. B.* 25: 2192–2206.

Arnott, S., and D. W. L. Hukins. 1972. Optimized parameters for A-DNA and B-DNA. *Biochem. Biophys. Res. Commun.* 47:1504–1509.

Arnott, S., and D. W. L. Hukins. 1973. Refinement of the structure of B-DNA and implications for the analysis of X-ray diffraction data from fibers of biopolymers. *J. Mol. Biol.* 81:93–105.

Arnott, S., and E. Selsing. 1975. The conformation of C-DNA. *J. Mol. Biol.* 98:265–269.

Balendiran, K., S. T. Rao, C. Y. Sekharudu, G. Zon, and M. Sundaralingam. 1995. X-ray structures of the B-DNA dodecamer d(CGCGTTAACGCG) with an inverted central tetranucleotide and its netropsin complex. *Acta Crystallogr. D.* 51:190–198.

Blümich, B., C. Böffel, G. S. Harbison, Y. Yang, and H. W. Spiess. 1987. Two-dimensional MAS NMR: new prospects for the investigation of partially oriented polymers. *Ber. Bunsenges. Phys. Chem.* 91: 1100–1103.

Brahms, J., J. Pilet, T. T. P. L. Lan, and L. R. Hill. 1973. Direct evidence of the C-like form of sodium deoxyribonucleate. *Proc. Natl. Acad. Sci. U.S.A.* 70:3352–3355.

Brandes, R., R. R. Vold, D. R. Kearns, and A. Rupprecht. 1988a. Static disorder and librational motions of the purine bases in films of oriented Li-DNA. *J. Mol. Biol.* 202:321–332.

Brandes, R., R. R. Vold, D. R. Kearns, and A. Rupprecht. 1988b. A ^{2}H-NMR study of the A-DNA conformation in films of oriented Na-DNA: evidence of a disordered B-DNA contribution. *Biopolymers.* 27:1159–1170.

Chandrasekaran, R., and S. Arnott. 1996. The structure of B-DNA in oriented fibers. *J. Biomol. Struct. Dyn.* 13:1015–1027.

Chandrasekaran, R., M. Wang, R. G. He, L. C. Puigjaner, M. A. Byler, R. P. Millane, and S. Arnott. 1989. A re-examination of the crystal

structure of A-DNA using fiber diffraction data. *J. Biomol. Struct. Dyn.* 6:1189–1202.

Coll, M., J. Aymami, G. A. van der Marel, J. H. van Boom, A. Rich, and A. H.-J. Wang. 1989. Molecular structure of the netropsin-(dCGCGATATCGCG) complex: DNA conformation in an alternating AT segment. *Biochemistry.* 28:310–320.

Ernst, R. R., G. Bodenhausen, and A. Wokaun, A. 1987. Principles Of Nuclear Magnetic Resonance in One and Two Dimensions. Clarendon Press, Oxford.

Falk, M. 1966. A gravimetric study of hydration of polynucleotides. *Can. J. Chem.* 44:1107–1111.

Flanagan, M. E., S. B. Rollins, and R. M. Williams. 1995. Netropsin and spermine conjugates of a water-soluble quinocarcin analog: analysis of sequence-specific DNA interactions. *Chem. Biol.* 2:147–156.

Fritzsche, H. 1994. Infrared linear dichroism studies of DNA-drug complexes: quantitative determination of the drug-induced restriction of the B-A transition. *Nucleic Acids Res.* 22:787–791.

Fritzsche, H., R. Brandes, A. Rupprecht, Z. Song, T. Weidlich, and D. R. Kearns. 1992. The formation of A-DNA in NaDNA films is suppressed by netropsin. *Nucleic Acids Res.* 20:1223–1228.

Fritzsche, H., M. Richter, and A. Rupprecht. 1984b. Restriction of conformational transitions of DNA in films induced by intercalating and non-intercalating antibiotics. *Stud. Biophys.* 104:91–95.

Fritzsche, H., A. Rupprecht, and M. Richter. 1984a. Infrared linear dichroism of oriented DNA-ligand complexes prepared with the wet-spinning method. *Nucleic Acids Res.* 12:9165–9177.

Fujiwara, T., and H. Shindo. 1985. Phosphorus-31 nuclear magnetic resonance of highly oriented DNA fibers. 2. Molecular motions in hydrated DNA. *Biochemistry.* 24:896–902.

Fuller, W., M. H. F. Wilkins, H. R. Wilson, and L. D. Hamilton. 1965. The molecular configuration of deoxyribonucleic acid. IV. X-ray diffraction study of the A form. *J. Mol. Biol.* 12:60–80.

Gabriëlse, W., H. F. J. M. van Well, and W. S. Veeman. 1996. Determination of the ^{13}C magnetic shielding tensor in partially oriented polymer systems. *Solid State Nucl. Magn. Reson.* 6:231–240.

Goodsell, D. S., M. L. Kopka, and R. E. Dickerson. 1995. Refinement of netropsin bound to DNA: bias and feedback in electron density map interpretation. *Biochemistry.* 34:4983–4993.

Harbison, G. S., and H. W. Spiess. 1986. Two-dimensional magic-angle-spinning NMR of partially ordered systems. *Chem. Phys. Lett.* 124: 128–134.

Harbison, G. S., V.-D. Vogt, and H. W. Spiess. 1987. Structure and order in partially oriented solids: characterization by 2D-magic-angle-spinning NMR. *J. Chem. Phys.* 86:1206–1218.

Heinemann, U., C. Alings, and M. Hahn. 1994. Crystallographic studies of DNA helix structure. *Biophys. Chem.* 50:157–167.

Herzfeld, J., R. G. Griffin, and R. A. Haberkorn. 1978. Phosphorus-31 chemical-shift tensors in barium diethyl phosphate and urea-phosphoric acid: model compounds for phospholipid head-group studies. *Biochemistry.* 14:2711–2718.

Juang, C. L., P. Tang, and G. S. Harbison. 1995. Solid-state NMR of DNA. *Nucl. Magn. Res.* 261:256–270.

Kopka, M. L., C. Yoon, D. Goodsell, P. Pjura, and R. E. Dickerson. 1985a. The molecular origin of DNA-drug specificity in netropsin and distamycin. *Proc. Natl. Acad. Sci. U.S.A.* 82:1376–1380.

Kopka, M. L., C. Yoon, D. Goodsell, P. Pjura, and R. E. Dickerson. 1985b. Binding of antitumor drug to DNA. Netropsin and C-G-C-G-A-A-T-T-^{Br}C-G-C-G. *J. Mol. Biol.* 183:553–563.

Langridge, R., H. R. Wilson, C. W. Hooper, M. H. F. Wilkins, and L. D. Hamilton. 1960. The molecular configuration of deoxyribonucleic acid. I. X-ray diffraction study of a crystalline form of the lithium salt. *J. Mol. Biol.* 2:19–37.

Maricq, M. M., and J. S. Waugh. 1979. NMR in rotating solids. *J. Chem. Phys.* 70:3300–3316.

Marvin, D. A., M. Spencer, M. H. F. Wilkins, and L. D. Hamilton. 1961. The molecular configuration of deoxyribonucleic acid. III. X-ray diffraction study of the C form of the lithium salt. *J. Mol. Biol.* 3:547–565.

Nall, B. T., W. P. Rothwell, J. S. Waugh, and A. Rupprecht. 1981. Structural studies of A-form sodium DNA: phosphorous-31 nuclear magnetic resonance of oriented fibers. *Biochemistry.* 20:1881–1887.

Patel, D. J., and L. Shapiro. 1985. Molecular recognition in noncovalent antitumor agent-dna complexes: NMR studies of the base and sequence dependent recognition of the DNA minor groove by netropsin. *Biochemie.* 67:887–915.

Pilet, J., and J. Brahms. 1972. Dependence of B-A conformational change in DNA on base composition. *Nature New Biol.* 236:99–100.

Pohle, W., and H. Fritzsche. 1984. Restriction of DNA conformational flexibility induced by antibiotics and amino compounds. *Stud. Biophys.* 104:303–308.

Pohle, W., V. B. Zhurkin, and H. Fritzsche. 1984. The DNA phosphate orientation. Infrared data and energetically favorable structures. *Biopolymers.* 23:2603–2622.

Premilat, S., and G. Albiser. 1983. Conformations of A-DNA and B-DNA in agreement with fiber X-ray and infrared dichroism. *Nucleic Acids Res.* 11:1897–1908.

Rhee, Y., C. Wang, B. L. Gaffney, and R. A. Jones. 1993. Nitrogen-15-labeled oligodeoxynucleotides. 6. Use of N-15 NMR to probe binding of netropsin and distamycin to $(d[CGCGAATTCGCG])_2$. *J. Am. Chem. Soc.* 115:8742–8746.

Rupprecht, A. 1966. Preparation of oriented DNA by wet spinning. *Acta Chem. Scand.* 20:494–504.

Rupprecht, A. 1970. A wet spinning apparatus and auxiliary equipment suitable for preparing samples of oriented DNA. *Biotechnol. Bioeng.* 12:93–121.

Rupprecht, A., and B. Forslind. 1970. Variation of electrolyte content in wet-spun lithium- and sodium-DNA. *Biochim. Biophys. Acta.* 204: 304–316.

Rupprecht, A., L. Nordenskiöld, L. Einarsson, J. Schultz, C. S. Huldt, and G. Lahajnar. 1991. Preparation of oriented Ca-DNA and Mg-DNA by means of the wet spinning method. *Acta Chem. Scand.* 45:216–218.

Rupprecht, A., J. Piskur, J. Schultz, L. Nordenskiöld, Z. Song, and G. Lahajnar. 1994. Mechanochemical study of conformational transitions and melting of Li-, Na-, K-, and CsDNA fibers in ethanol-water solutions. *Biopolymers.* 34:897–920.

Saenger, W. 1984. Principles of Nucleic Acid Structure. Springer, New York.

Schmidt-Rohr, K., and H. W. Spiess. 1994. Multidimensional Solid-State NMR and Polymers. Academic Press, London.

Schultz, J., A. Rupprecht, Z. Song, J. Piskur, L. Nordenskiöld, and G. Lahajnar. 1994. A mechanochemical study of MgDNA fibers in ethanol-water solutions. *Biophys. J.* 66:810–819.

Shindo, H., T. Fujiwara, H. Akutsu, U. Matsumoto, and Y. Kyogoku. 1985. Phosphorus-31 nuclear magnetic resonance of highly oriented DNA fibers. 1. Static geometry of DNA double helices. *Biochemistry.* 24: 887–895.

Song, Z. Y., O. N. Antzutkin, A. Rupprecht, and M. H. Levitt. 1996. Order-resolved sideband separation in magic-angle-spinning NMR. ^{31}P-NMR of oriented DNA fibers. *Chem. Phys. Lett.* 253:349–354.

Tabernero, L., N. Verdaguer, M. Coll, I. Fita, G. A. van der Marel, J. H. van Boom, A. Rich, and J. Aymamí. 1993. Molecular structure of the A-tract DNA dodecamer d(CGCAAATTTGCG) complexed with the minor groove binding drug netropsin. *Biochemistry.* 32:8403–8410.

Tang, P., C.-L. Juang, and G. S. Harbison. 1990. Intercalation complex of proflavine with DNA: structure and dynamics by solid-state NMR. *Science.* 249:70–72.

Tang, P., R. A. Santos, and G. S. Harbison. 1989. Two-dimensional solid-state nuclear magnetic resonance studies of the conformation of oriented DNA. *Advan. Magn. Res.* 13:225–255.

Varshalovich, D. A., A. N. Moskalev, and V. K. Khersonskii. 1988. Quantum Theory of Angular Momentum. World Scientific Publishing, Singapore.

Wahl, M. C., and M. Sundaralingam. 1995. New crystal structures of nucleic acids and their complexes. *Curr. Opin. Struct. Biol.* 5:282–295.

Wartell, R. M., J. E. Larson, and R. D. Wells. 1974. Netropsin: a specific probe for A-T regions of duplex deoxyribonucleic acid. *J. Biol. Chem.* 249:6719–6731.